Journal of Physical Chemistry and Functional Materials

Home Page of Journal: https://dergipark.org.tr/jphcfum

Effect of Heat Treatment on Some Thermodynamics Analysis, Crystal and Microstructures of Cu-Al-X (X: Nb, Hf) Shape Memory Alloy

Ecem Özen Öner[1], Gonca Ateş[2], Safar Saeed Mohammed*[3] M. Sait Kanca[4], Mediha Kök[1]

[1]Department of Physics, Faculty of Science, Firat University, Elazig, Turkey
[2]Department of Medical Services and Techniques, Sirnak University, Sirnak, Turkey
[3]Department of General and Applied Physics, College of Science, University of Raparin, Sulaymaniyah, Iraq
[4]Rare Earth Elements Application and Research Center, Munzur University, Tunceli, Turkey
** Corresponding author: E-mail: safar.saeed@uor.edu.krd*

ABSTRACT

In recent years, nuclear power plants have been built worldwide. This amount large of power is better than other energy sources for the environment, it does not have a greenhouse gas. A pressurized water reactor (PWR) is a type of light water reactor to generate electricity and it needed enriched Uranium and large cost. The purpose of this work was to investigate three different types of steel for PWR reactor vessels such as SA30400, SA302B and SA355B-1 steel. The result shows that SA355B-1 performs better than the other. On the other hand, phonons, ionization and collision events show very little damage to all materials.

ARTICLE INFO

Keywords:
Shape memory alloy
Heat Treatment
Microstructures
Cu-Al-Nb
Cu-Al-Hf

Received: 2024-05-11
Accepted: 2024-05-28
ISSN: 2651-3080
DOI: **10.54565/jphcfum.1482215**

Introduction

Shape memory alloys discovered by Arne Ölander in the 1930s were explained by Vernom in the 1940s [1, 2]. The shape memory effect of shape memory alloys was determined in the alloy formed by combining gold and cadmium elements in the studies conducted in the 1950s. Then, they determined the importance of the shape memory effect of shape memory alloys in Nickel-Titanium alloy made by William Buehler and Frederick Wank in 1962 [3]. The most commonly used shape memory alloys today are copper-based ones because they are less costly than nickel-based ones [4]. The reason why shape memory alloys have gained importance in recent years is that they are advanced functional smart materials [5-10]. Smart materials are materials whose chemical composition and physical state change [11, 12]. They have physical (optical, magnetic, electrical, and mechanical) or physicochemical (rheological) properties that can change significantly with external factors such as pressure, temperature, humidity, pH, electric or magnetic field. Smart materials are called “smart” because of this property of materials such as some external sensors, or actuators that perform a certain action when actuated by a control signal [13-17]

These smart materials are functional materials capable of regaining their original shape and size when heated to high temperatures (austenite phase region) Af upon application of low (martensite phase) cooling or stress and show a reversible thermoelastic martensitic transformation [18-20]. Shape memory alloys are widely used in various industrial applications, the automotive industry, aerospace studies, robotic applications, and the surgical-biomedical industry. Copper-based and nickel-based shape memory alloys are the most commonly used. NiTi alloy is used especially in areas that need to be biocompatible. However, due to the high cost of NiTi alloys and their relatively low transformation temperatures, they are not useful as damping materials at moderate temperatures [21, 22]. Copper-based alloys are preferred for their low cost, ease of manufacture and machinability, lower hysteresis and higher conversion temperatures [23-25].

Stipcich. et al. have argued that the third element additive increases the thermal stability, brittleness, mechanical elasticity, grain size of the alloy, has high elastic anisotropy or creates an impurity or a second phase at the grain boundary [26]. Alaneme K. et al. observed that the third element to be added to Cu-Zn and Cu-Al alloys in copper-based alloys change the transformation temperatures and microstructure [27].

The aim of the study was to produce two different CuAl based shape memory alloys by adding Nb, and Hf elements in the same mass ratio to the $Cu_{86}Al_{12}Nb_x$, $Cu_{86}Al_{12}Hf_x$ (x=2 wt.%). The shape memory effect in the produced alloys was investigated by looking at the crystal and microstructure and thermal properties of the alloys. It was thought that adding a third element to this copper-based study would affect various physical properties.

2. Experimental Procedure

2.1. Materials and Productions

In this study, two CuAl-based shape memory alloys were used. Mass ratios of alloys are given in Table 1. High purity powder elements prepared according to Table 1 were pelletized under pressure. The alloy powders brought to the pellet were produced by arc melting method under vacuum and the produced alloys were kept at 900 °C for 24 hours to ensure their homogeneity.

Table 1. Chemical composition in CuAlX (X: Nb, Hf) (% mass) alloys

Sample	Cu(%mass)	Al(%mass)	Nb(%mass)	Hf(%mass)
Nb	86	12	2	-
Hf	86	12	-	2

2.2. Characterization Process

The produced alloy samples were heat treated at 973 K, 1073 K and 1173 K for one hour, and after the heat treatment, they were suddenly cooled in salty ice water. After heat treatment, the change in the thermal properties of the samples was determined using DSC (Differential Scanning calorimetry). The changes caused by the heat treatment on the crystal and microstructure of the alloy samples were determined at room temperature using X-ray (XRD), Scanning Electron microscopy (SEM) device and optical microscope.

3. Results and Discussion

3.1. Thermal Analysis Results

The DSC measurements were carried out for thermal analysis of $Cu_{86}Al_{12}Nb_2$ and $Cu_{86}Al_{12}Hf_2$ (mass %) after heat treatment of both samples in three different temperatures (973 K, 1073 K and 1173 K). Figure 1 represents the typical curves of DSC. According to Figure 1, both samples are in the austenite phase at room temperature. Also, the transformation temperatures including austenite start (As), austenite finish (Af), martensite start (Ms), martensite finish (Mf) were tabulated in Table 2. According to Table 2 both $Cu_{86}Al_{12}Nb_2$ and $Cu_{86}Al_{12}Hf_2$ (wt. %) samples can be called high-temperature SMAs (HTSMAs) because the phase transition process (martensite ⇆ austenite) were occurred above 100 °C (373 K) [28]. Also, Figure 2-(a) shows the effect of heat treatment on the transformation temperatures (TTs) of both $Cu_{86}Al_{12}Nb_2$ and $Cu_{86}Al_{12}Hf_2$ (mass %) alloys. According to Figure2 -(a) all TTs were affected by heat treatment which both ***Af*** and ***Mf*** were decreased by increasing the treatment temperature in both samples, while ***Ms*** was increased, but ***As*** was different in both samples that in Cu86Al12-Nb2 (mass %) it was increased but in Cu86Al12-Hf2 (mass %) was decreased. Figure 2-(b) shows the calculated temperature hysteresis of heat treated samples that it can be seen that in both samples ($Cu_{86}Al_{12}Nb_2$ and $Cu_{86}Al_{12}Hf_2$ (mass %)) the increase in treatment temperature caused to decrease the temperature hysteresis.

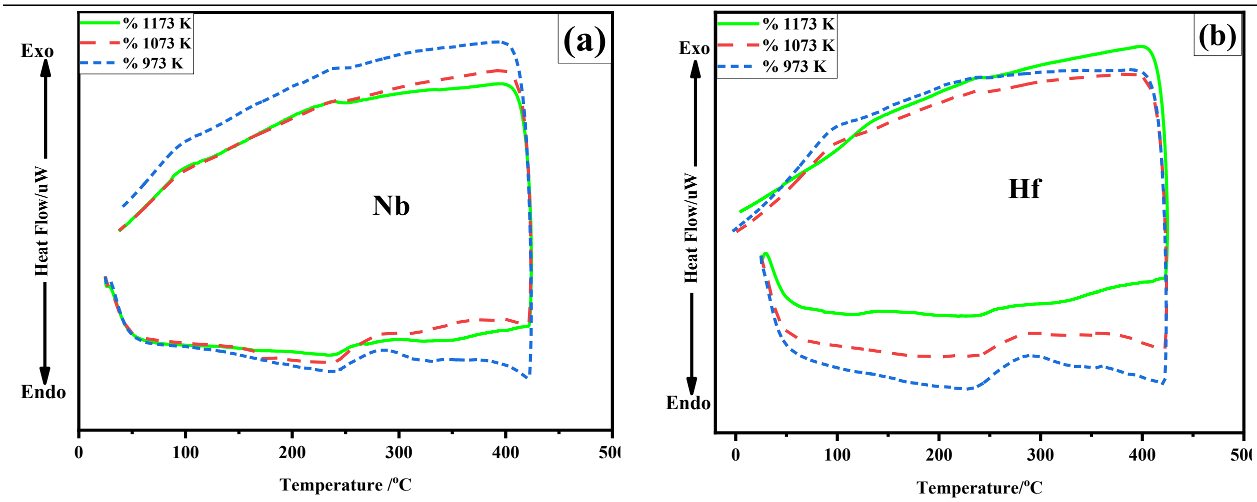

Fig.1. DSC curves of (a) $Cu_{86}Al_{12}$-Hf_2 and (b) $Cu_{86}Al_{12}$-Nb_2 (wt. %) heat treated alloy samples

Table 2. Transformation temperatures for all treated alloys

Sample	As / K	Af / K	Ms / K	Mf / K
Nb-973 K	572.9	635.9	558.6	513.3
Nb-1073 K	574.2	634	568.8	506.1
Nb-1173 K	577.6	614.3	591.2	502.6
Hf-973 K	566.4	624.7	556	502.2
Hf-1073 K	557.3	631.3	561.4	501.7
Hf-1173 K	544.7	610.4	562.8	500

The heat change through the heating and cooling processes (or enthalpy change in both forward ($\Delta H^{M\to A}$) and reverse ($\Delta H^{A\to M}$) martensitic transformation was obtained based on the DSC curves which is equal to the area under the DSC curves. In the other word enthalpy change can be calculated as follows [29]:

$$\Delta H^{M\to A} = \int_{A_s}^{A_f} \frac{dq}{dt}\left(\frac{dT}{dt}\right)^{-1} dT \quad , \quad \Delta H^{A\to M} = \int_{A_f}^{A_s} \frac{dq}{dt}\left(\frac{dT}{dt}\right)^{-1} dT \qquad (1)$$

Where (q) is the heat absorbed by the sample, (T) is the absolute temperature, and (t) is the time.

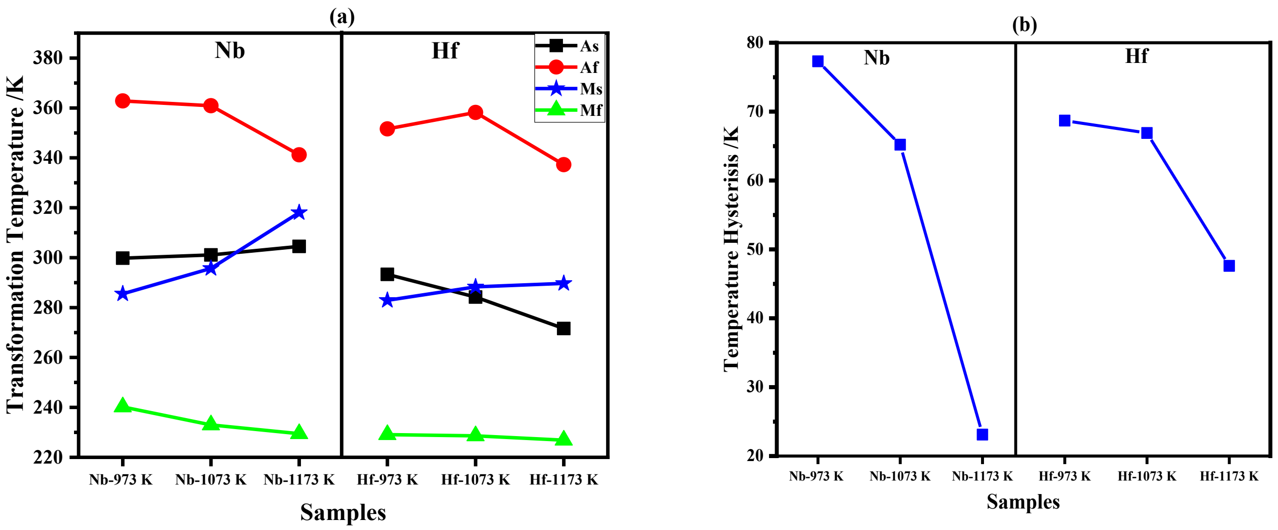

Fig 2. (a) Phase transformation temperatures and **(b)** Temperature hysteresis of both $Cu_{86}Al_{12}Nb_2$ and $Cu_{86}Al_{12}Hf_2$ (wt. %) heat treated alloys

Another thermodynamics parameter is entropy change (ΔS) which is the disorderness of the microstructure of the alloy system. And it can be calculated by the following equation [30]:

$$\Delta S^{M\to A} = \frac{\Delta H^{M\to A}}{T_o} \quad , \quad \Delta S^{A\to M} = \frac{\Delta H^{A\to M}}{T_o} \qquad (2)$$

Where T_o is the equilibrium temperature. The value of T_o was defined as follows [31]:

$$T_o = \frac{M_s + A_f}{2} \quad (3)$$

Also, T_o can be defined in such a way that the Gibbs free energy in both forward ($\Delta G^{M\to A}(T_o)$) and reverse ($\Delta G^{A\to M}(T_o)$) martensitic transformations is equal to zero. In the other words the Gibbs free energy in both forward ($\Delta G^{M\to A}(T_o)$) and reverse ($\Delta G^{A\to M}(T_o)$) martensitic transformation can be calculated as these to following equations [32, 33]:

$$\Delta G^{M\to A}(T_o) = G^A(T_o) - G^M(T_o) = (H^A - T_o S^A) - (H^M - T_o S^M) = \Delta H^{M\to A} - T_o \Delta S^{M\to A} = 0 \quad (4)$$

$$\Delta G^{A\to M}(T_o) = G^M(T_o) - G^A(T_o) = (H^M - T_o S^M) - (H^A - T_o S^A) = \Delta H^{A\to M} - T_o \Delta S^{A\to M} = 0 \quad (5)$$

In addition, the elastic energy can be obtained by subtracting the Gibbs free energy in both M_s and M_f as follow:

$$G_e = \Delta G^{A\to M}(M_s) - \Delta G^{A\to M}(M_f) = (M_s - M_f)\,\Delta S^{M\to A} \quad (6)$$

Depending on equation (1- 6) all calculated thermodynamic parameters such as enthalpy change (ΔH), entropy change (ΔS), equilibrium temperature (T_o), Gibbs free energy (ΔG) and elastic energy (G_e) were tabulated in table 2 and graphically were shown in Figure 3 and Figure 4.

According to Table 2 and Figure 3, both enthalpy change and entropy change have the same pattern which were affected by increasing the treated temperature. As shown in Figure 3 (a), in $Cu_{86}Al_{12}Nb_2$ (mass %) enthalpy change increased by increasing treated temperature in forward martensitic transformation while it was decreased in reverse martensitic transformation. But in $Cu_{86}Al_{12}Hf_2$it was diminished in both the forward and reverse process. And in Figure 3 (b) can be seen that the treated temperature has the same effect on entropy as it has on enthalpy in both samples.

Table 3. Calculated thermodynamic factors for all treated samples.

Samples	T_o (K)	$\Delta G^{A\to M}$ (J.kg^{-1})	G_e (J.kg^{-1})	$\Delta S^{A\to M}$ (J.kg^{-1}.K^{-1})	$\Delta S^{M\to A}$ (J.kg^{-1}.K^{-1})	$\Delta H^{M\to A}$ (J.g^{-1})	$\Delta H^{A\to M}$ (J.g^{-1})
Nb-973 K	597.25	58.24	68.26	0.00194	0.00151	0.9	1.16
Nb-1073 K	601.4	164.24	315.90	0.00170	0.00504	3.03	1.02
Nb-1173 K	602.75	59.21	454.21	0.00146	0.00513	3.09	0.88
Hf-973 K	590.35	148.37	232.39	0.00256	0.00432	2.55	1.51
Hf-1073 K	596.35	69.15	118.13	0.00211	0.00198	1.18	1.26
Hf-1173 K	586.6	42.19	111.34	0.00191	0.00177	1.04	1.12

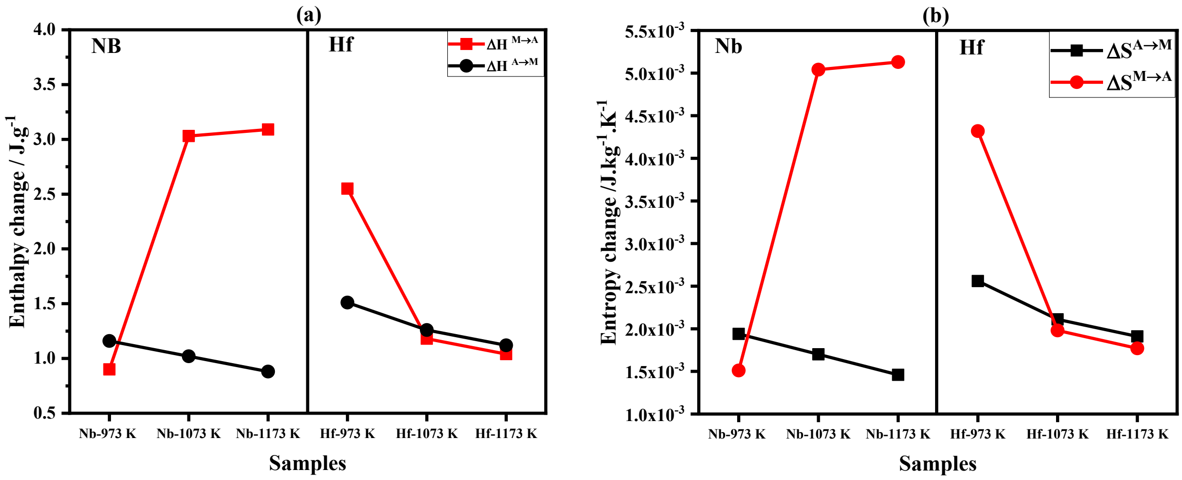

Fig 3. (a) Enthalpy change and (b) Entropy change in both forward and reverse martensitic transformation of $\mathbf{Cu_{86}Al_{12}Nb_2}$ and $\mathbf{Cu_{86}Al_{12}Hf_2}$ (wt. %) heat treated alloys

The treated temperature has a different effect on Gibbs free energy (ΔG) in each sample (Figure 4 (a), which is caused to increase the Gibbs free energy (ΔG) in $Cu_{86}Al_{12}Nb_2$ by a different amount, but Gibbs free energy (ΔG) was reduced regularly in $Cu_{86}Al_{12}Hf_2$ by increasing treated temperature. In addition, Figure 4 (b) represents that the treated temperature has the same effect on elastic energy as it has on Gibbs free energy which is cased to increase the elastic energy in $Cu_{86}Al_{12}Nb_2$ while it decreased elastic energy in $Cu_{86}Al_{12}Hf_2$. Also, M. Kok et al. were found the same result in their study, that they were determined that the elastic energy of Ni-Ti-V alloy decreased when the heat treatment temperature was increased [21].

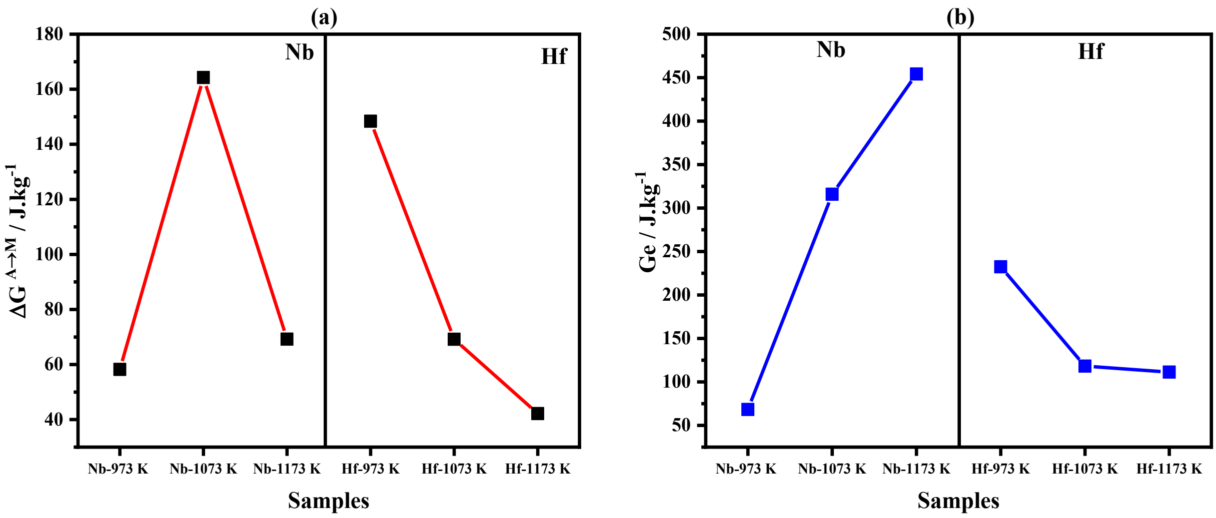

Fig 4. (a) Gibbs free energy (b) Elastic energy in both forward and reverse martensitic transformation of $Cu_{86}Al_{12}Nb_2$ and $Cu_{86}Al_{12}Hf_2$ (wt. %) heat treated alloys**.**

3.2. Crystallinity Results

Figure 5 shows the XRD pattern measurement after heat treatment at 973 K and 1173 K which was taken at room temperature. The peaks were indexed by using the literature [29, 34, 35].In Figure 5 can be seen that in all cases the main peaks are both Cu and Al peaks in both $Cu_{86}Al_{12}Nb_2$ (mass %) and $Cu_{86}Al_{12}Hf_2$ (mass %) samples. Also, the Cu-Al peak was indicated as a precipitate. And in the $Cu_{86}Al_{12}Nb_2$ sample the intensity of peaks decreased by increasing the treated temperature, while in $Cu_{86}Al_{12}Hf_2$ (mass %) the intensity in all peaks did not change after raising the temperature. Also, in $Cu_{86}Al_{12}Hf_2$ (mass %) the number of Al peaks were decreased by increasing the temperature because some of them were disappeared.

The crystallite size of obtained alloys was calculated by the Debye Scherer equation as follow [36]:

$$D = \frac{K\lambda}{B\cos\theta} \quad (7)$$

Where K is the shape factor (K=0.9), λ is the wavelength of incident X-Ray (λ =1.5406 Å), B is the full-width half maximum of the XRD peaks (FWHM), and θ is the Braggs angle [28]. Figure 6 represents the calculated crystallite size of both $Cu_{86}Al_{12}Nb_2$ and $Cu_{86}Al_{12}Hf_2$ (mass %). According to Figure 6, the crystallite size of $Cu_{86}Al_{12}Hf_2$was increased by increasing the treated temperature, while it was decreased in $Cu_{86}Al_{12}Nb_2$ (mass %).

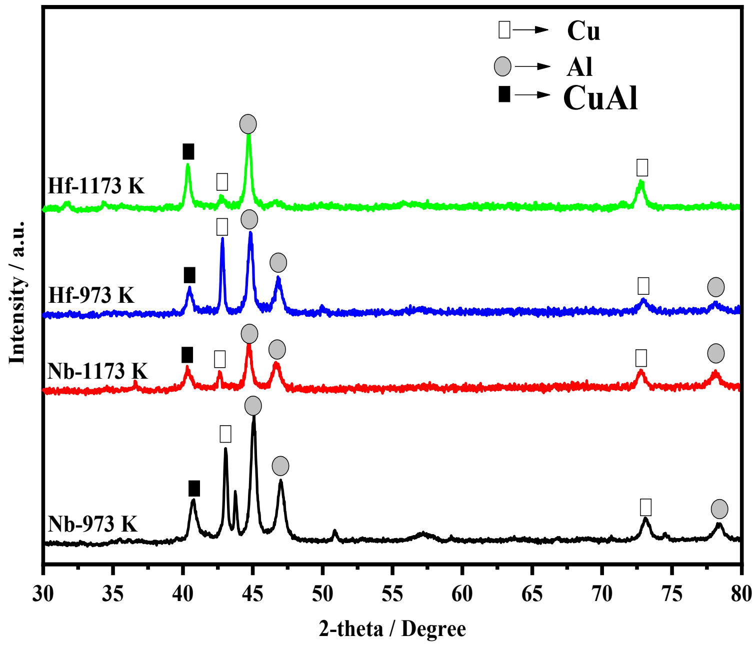

Fig 5. The XRD measurement result for of $Cu_{86}Al_{12}Nb_2$ and $Cu_{86}Al_{12}Hf_2$ (wt. %) shape memory alloys.

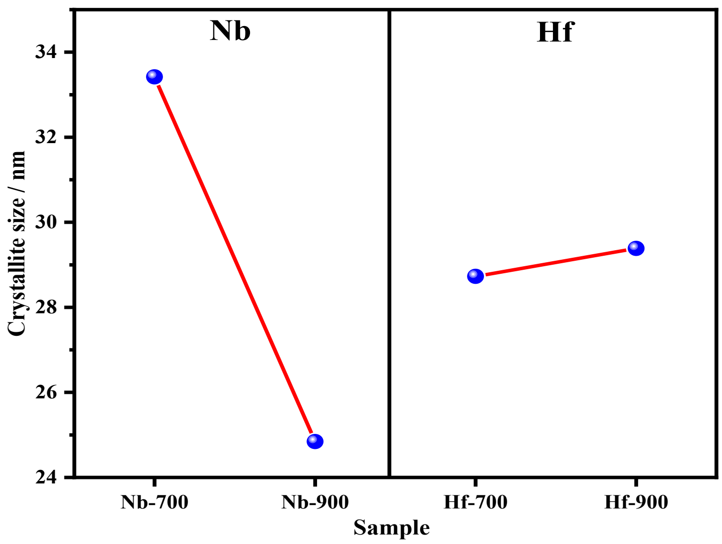

Fig 6. Calculated crystallite size of $Cu_{86}Al_{12}Nb_2$ and $Cu_{86}Al_{12}Hf_2$ (wt. %) heat treated alloys

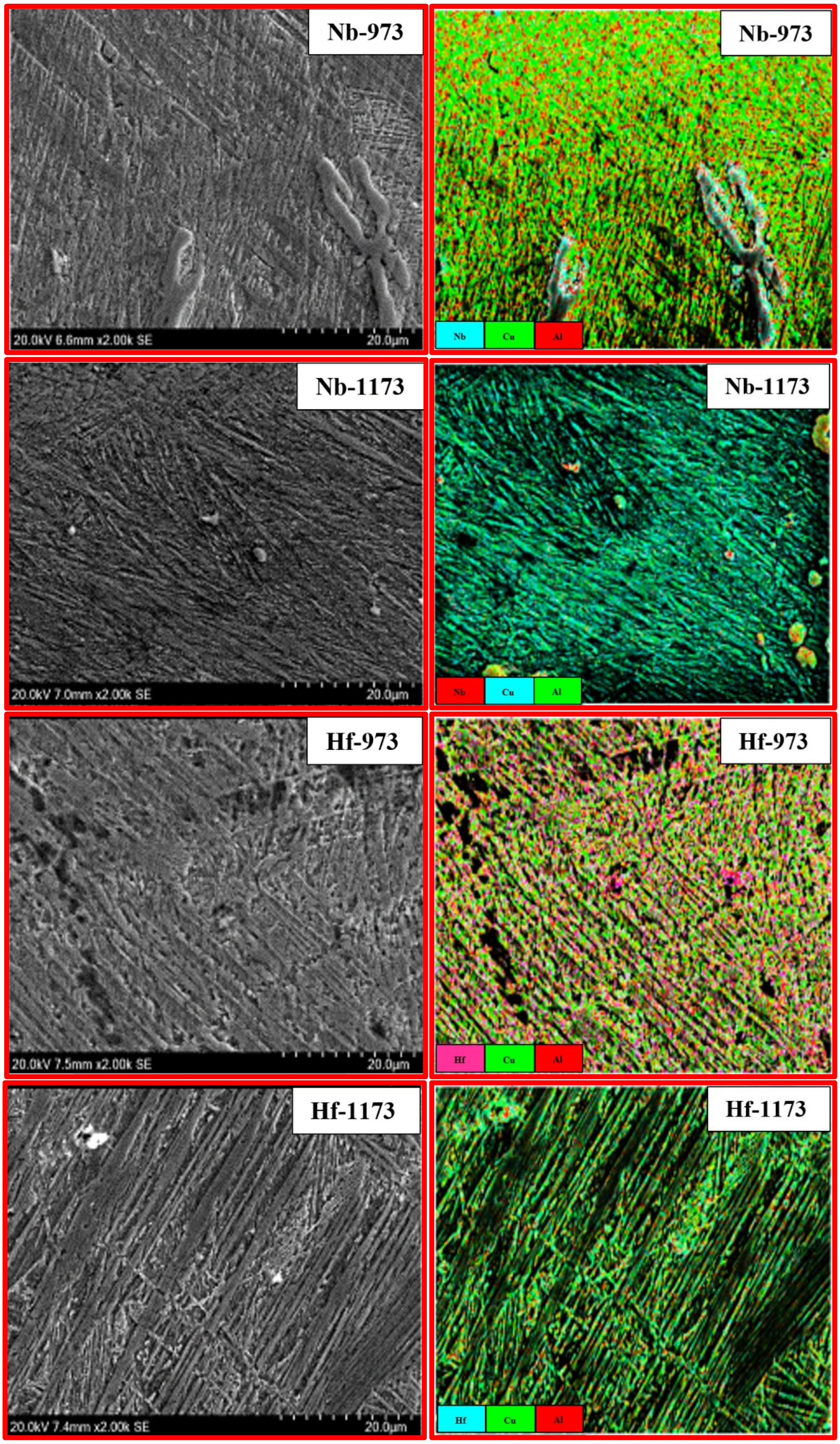

Figure 7. SEM images (left side) and mapping images (right side) for $Cu_{86}Al_{12}Nb_2$ and $Cu_{86}Al_{12}Hf_2$ (wt. %) heat treated alloys.

3.3. Microstructure analysis

Figure 7 represents the SEM analysis results (left side) and the mapping images (right side). Information on the constituents is provided from the maps. In figure 7 appears that Hf is more dissolved in the alloy compared to Nb. Because the Nb has accumulated in some areas on the alloy matrix and has settled as an impurity separately. But by increasing the temperature, it melts further into the alloy. While Hf appears to be less settled as an impurity and most of its amount is dissolved in the alloy.

3.4. Optical Microscope Images

The optical microscope images agree with the SEM images, which is observed that at low temperatures, the Nb content in $Cu_{86}Al_{12}Nb_2$ did not dissolve completely in the alloy, and it spreads in the form of small flowers on the alloy's surface, but it was dissolved by increasing the treated temperature. And the Hf was dissolved in both low and high temperatures in $Cu_{86}Al_{12}Hf_2$.

Also, Figure 8 shows that in $Cu_{86}Al_{12}Nb_2$ the size of grains was decreased by increasing temperature, while $Cu_{86}Al_{12}Hf_2$ they were increased. And this result is supported by calculated grain size results in Figure 6.

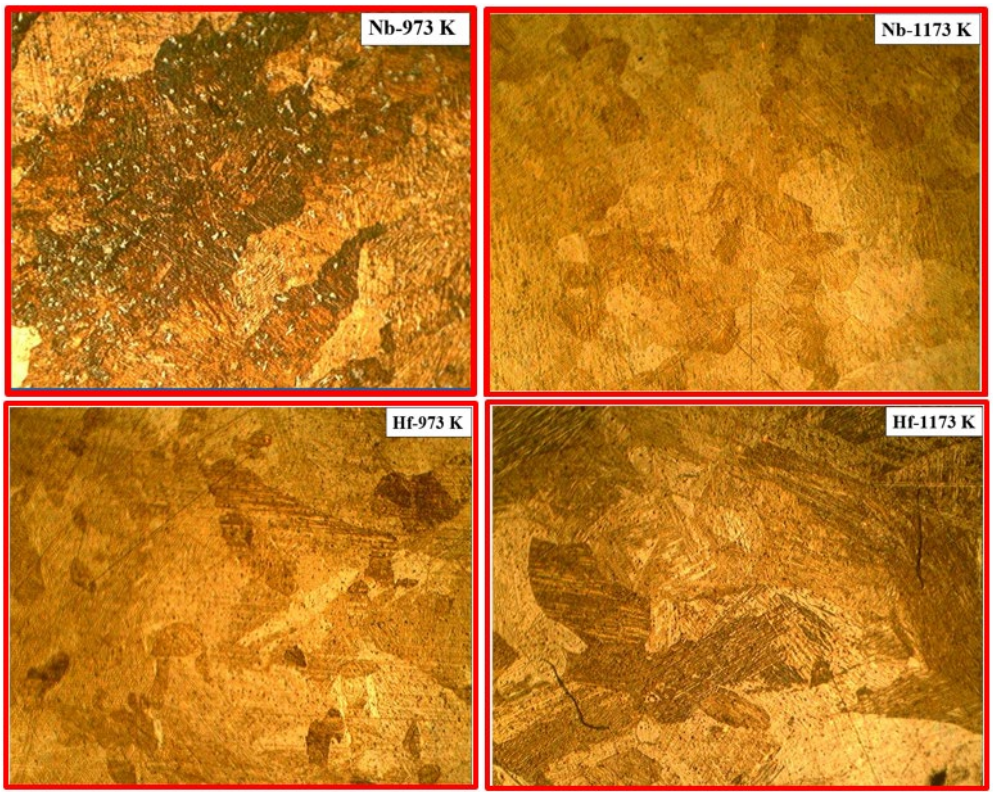

Fig. 8. Optical images of all sample alloys.

Conclusions

In this study the effect of heat treatment at three different temperatures (973 K, 1073 K and 1173 K) on some thermodynamics parameters, crystal structure, and microstructure of $Cu_{86}Al_{12}Nb_2$ and $Cu_{86}Al_{12}Hf_2$ (mass %) Shape Memory Alloy has been investigated. The main important results were summarized as follow:

- Both $Cu_{86}Al_{12}Nb_2$ and $Cu_{86}Al_{12}Hf_2$ (mass %) samples can be called high-temperature SMAs (HTSMAs) because the phase transition process (martensite ⇆ austenite) have occurred above 100 °C (373 K)
- Both Af and Mf were decreased by increasing the treatment temperature in both samples, while Ms was increased, but As was different in both samples that in $Cu_{86}Al_{12}Nb_2$ (mass %) it was increased but in $Cu_{86}Al_{12}Hf_2$ (mass %) was decreased.
- In both samples ($Cu_{86}Al_{12}Nb_2$ and $Cu_{86}Al_{12}Hf_2$ (mass %)) the increase in treatment temperature caused to decrease the temperature hysteresis.
- Heat treatment has further stabilized both samples since in both samples the entropy change which is the disorderness of the thermodynamic system has been decreased.
- According to XRD and optical microimages, the size of grains was decreased in $Cu_{86}Al_{12}Nb_2$ but it was increased in $Cu_{86}Al_{12}Hf_2$.
- SEM result shows that Hf is more dissolved in the alloy compared to Nb. Because the Nb has accumulated in some areas on the alloy matrix and has settled as an impurity separately. But by increasing the temperature, it melts further into the alloy. While Hf

appears to be less settled as an impurity and most of its amount is dissolved in the alloy.

Acknowledgments

E. Özen Öner *MSc*. is supporting by the Council of Higher Education-Turkey (CoHE) with 100/2000 Ph.D. Scholarship. This work was supported by the Management Unit of the Scientific Research Projects of Firat University-Turkey (FUBAP) (Project Numbers: FF.21.32).

References

[1] M. Elahinia, M. T. Andani and C. Haberland. Shape memory and superelastic alloys. *High Temperature Materials and Mechanisms*. 2014;355.

[2] G. Dennis, J. Santos, C. S. Kiminami and P. Gargarella. Comparison of Cu–Al–Ni–Mn–Zr shape memory alloy prepared by selective laser melting and conventional powder metallurgy. *Transactions of Nonferrous Metals Society of China*. 2020;30(12):3322-3332. doi:https://doi.org/10.1016/S1003-6326(20)65464-4.

[3] J. M. Jani, M. Leary and A. Subic, editors. Shape memory alloys in automotive applications. Applied Mechanics and Materials; 2014: Trans Tech Publ.

[4] V. Malik, S. Srivastava, S. Gupta, V. Sharma, M. Vishnoi and T. Mamatha. A novel review on shape memory alloy and their applications in extraterrestrial roving missions. *Materials Today: Proceedings*. 2021;44:4961-4965. doi:https://doi.org/10.1016/j.matpr.2020.12.860.

[5] S. Mohammed, M. Kök, Z. Çirak, I. Qader, F. Dağdelen and H. Zardawi. The relationship between cobalt amount and oxidation parameters in NiTiCo shape memory alloys. *Physics of Metals and Metallography*. 2020;121(14):1411-1417. doi:https://doi.org/10.1134/S0031918X2013013X.

[6] M. Schwartz. Smart materials. CRC press; 2008.

[7] S. S. Mohammed, M. KÖK, I. N. Qader and F. Dağdelen. The developments of piezoelectric materials and shape memory alloys in robotic actuator. *Avrupa Bilim ve Teknoloji Dergisi*. 2019(17):1014-1030.

[8] R. QADIR, S. MOHAMMED, M. KÖK and I. QADER. A review on NiTiCu shape memory alloys: manufacturing and characterizations. *Journal of Physical Chemistry and Functional Materials*. 2021;4(2):49-56.

[9] R. Qadır, S. Mohammed, M. Kök and I. Qader. A review on NiTiCu shape memory alloys: manufacturing and characterizations. *Journal of Physical Chemistry and Functional Materials*. 2021;4(2):49-56.

[10] S. S. Mohammed, M. Kök, I. Qader and R. Qadır. A Review on the Effect of Mechanical and Thermal Treatment Techniques on Shape Memory Alloys. *Journal of Physical Chemistry and Functional Materials*. 2022;5(1):51-61.

[11] C. Hsu, W. Wang, Y. Hsu and W. Rehbach. The refinement treatment of martensite in Cu–11.38 wt.% Al–0.43 wt.% Be shape memory alloys. *Journal of Alloys and Compounds*. 2009;474(1-2):455-462.

[12] K. Otsuka and X. Ren. Recent developments in the research of shape memory alloys. *Intermetallics*. 1999;7(5):511-528. doi:https://doi.org/10.1016/S0966-9795(98)00070-3.

[13] G. López, M. Barrado, E. Bocanegra, J. San Juan and M. Nó. Influence of the matrix and of the thermal treatment on the martensitic transformation in metal matrix composites. *Materials Science and Engineering: A*. 2008;481:546-550. doi:https://doi.org/10.1016/j.msea.2007.01.186.

[14] P. Kumar, A. K. Jain, S. Hussain, A. Pandey and R. Dasgupta. Changes in the properties of Cu-Al-Mn shape memory alloy due to quaternary addition of different elements. *Matéria (Rio de Janeiro)*. 2015;20:284-292. doi: https://doi.org/10.1590/S1517-707620150001.0028.

[15] I. N. Qader, E. Öner, M. Kok, S. S. Mohammed, F. Dağdelen, M. S. Kanca and Y. Aydoğdu. Mechanical and thermal behavior of Cu84−xAl13Ni3Hfx shape memory alloys. *Iranian Journal of Science and Technology, Transactions A: Science*. 2021;45(1):343-349. doi:https://doi.org/10.1007/s40995-020-01008-w.

[16] E. Balci, F. Dagdelen, S. Mohammed and E. Ercan. Corrosion behavior and thermal cycle stability of TiNiTa shape memory alloy. *Journal of Thermal Analysis and Calorimetry*. 2022;147(24):14953-14960.

[17] S. Mohammed, E. Balci, F. Dagdelen and S. Saydam. Comparison of Thermodynamic Parameters and Corrosion Behaviors of Ti50Ni25Nb25 and Ti50Ni25Ta25 Shape Memory Alloys. *Physics of Metals and Metallography*. 2022;123(14):1427-1435.

[18] T. Gustmann, J. Dos Santos, P. Gargarella, U. Kühn, J. Van Humbeeck and S. Pauly. Properties of Cu-based shape-memory alloys prepared by selective laser melting. *Shape Memory and Superelasticity*. 2017;3(1):24-36. doi:https://doi.org/10.1007/s40830-016-0088-6.

[19] T. R. K. Dora, V. Sampath, Y. Li and P. Hodgson. In vitro cytotoxicity and corrosion studies of some copper base shape memory alloys. *Materials Today: Proceedings*. 2017;4(10):10672-10681. doi:https://doi.org/10.1016/j.matpr.2017.08.013.

[20] B. M. IBRAHIM, S. S. MOHAMMED and E. BALCİ. A Review on Comparison between NiTi-Based and Cu-Based Shape Memory Alloys. *Journal of Physical Chemistry and Functional Materials*.6(2):40-50.

[21] M. Kök, A. O. A. Al-Jaf, Z. D. Çirak, I. N. Qader and E. Özen. Effects of heat treatment temperatures on phase transformation, thermodynamical parameters, crystal microstructure, and electrical resistivity of NiTiV shape memory

alloy. *Journal of Thermal Analysis and Calorimetry*. 2020;139(6):3405-3413. doi:https://doi.org/10.1007/s10973-019-08788-3.

[22] S. Mohammed, M. Kök, I. N. Qader and M. Coşkun. A review study on biocompatible improvements of NiTi-based shape memory alloys. *International Journal of Innovative Engineering Applications*. 2021;5(2):125-130.

[23] T. Elrasasi, M. Dobróka, L. Daróczi and D. Beke. Effect of thermal and mechanical cycling on the elastic and dissipative energy in CuAl (11.5 wt%) Ni (5.0 wt%) shape memory alloy. *Journal of Alloys and Compounds*. 2013;577:S517-S520. doi:https://doi.org/10.1016/j.jallcom.2012.06.108.

[24] M. Kok, R. A. Qadir, S. S. Mohammed and I. N. Qader. Effect of transition metals (Zr and Hf) on microstructure, thermodynamic parameters, electrical resistivity, and magnetization of CuAlMn-based shape memory alloy. *The European Physical Journal Plus*. 2022;137(1):62. doi:https://doi.org/10.1140/epjp/s13360-021-02297-9.

[25] S. S. M. Mohammed. Production and investigation of some physical properties of CuAlNiTa quaternary shape memory alloys: Fen Bilimleri Enstitüsü; 2021.

[26] M. Stipcich and R. Romero. β-Phase thermal degradation in Zr-added Cu–Zn–Al shape memory alloy. *Journal of Thermal Analysis and Calorimetry*. 2017;129(1):201-207. doi:https://doi.org/10.1007/s10973-017-6157-z.

[27] K. K. Alaneme and E. A. Okotete. Reconciling viability and cost-effective shape memory alloy options–A review of copper and iron based shape memory metallic systems. *Engineering Science and Technology, an International Journal*. 2016;19(3):1582-1592. doi:https://doi.org/10.1016/j.jestch.2016.05.010.

[28] S. S. Mohammed, M. Kok, I. N. Qader, M. S. Kanca, E. Ercan, F. Dağdelen and Y. Aydoğdu. Influence of Ta additive into Cu84− xAl13Ni3 (wt%) shape memory alloy produced by induction melting. *Iranian Journal of Science and Technology, Transactions A: Science*. 2020;44(4):1167-1175. doi:https://doi.org/10.1007/s40995-020-00909-0.

[29] M. Kök, I. N. Qader, S. S. Mohammed, E. Öner, F. Dağdelen and Y. Aydogdu. Thermal stability and some thermodynamics analysis of heat treated quaternary CuAlNiTa shape memory alloy. *Materials Research Express*. 2019;7(1):015702.

[30] F. Dagdelen, E. Balci, I. Qader, E. Ozen, M. Kok, M. Kanca, S. Abdullah and S. Mohammed. Influence of the Nb content on the microstructure and phase transformation properties of NiTiNb shape memory alloys. *JOM*. 2020;72(4):1664-1672. doi:https://doi.org/10.1007/s11837-020-04026-6.

[31] J. Ortin and A. Planes. Thermodynamic analysis of thermal measurements in thermoelastic martensitic transformations. *Acta metallurgica*. 1988;36(8):1873-1889. doi:https://doi.org/10.1088/2053-1591/ab5bef.

[32] S. S. Mohammed, E. Balci, H. A. Qadir, I. N. Qader, S. Saydam and F. Dagdelen. The exploring microstructural, caloric, and corrosion behavior of NiTiNb shape-memory alloys. *Journal of Thermal Analysis and Calorimetry*. 2022;147(21):11705-11713.

[33] S. Mohammed, M. Kök, Z. Çirak, I. Qader, F. Dağdelen and H. S. Zardawi. The relationship between cobalt amount and oxidation parameters in NiTiCo shape memory alloys. *Physics of Metals and Metallography*. 2020;121:1411-1417.

[34] M. da Silva, T. de Mello, A. Veloso and S. de Lima. Study of mechanical alloying in the obtention Cu-Al-Nb alloys with Shape Memory Effect. doi: https://doi.org/10.1590/S1516-14392005000200014.

[35] M. d. C. A. d. Silva and S. J. G. d. Lima. Evaluation of mechanical alloying to obtain Cu-Al-Nb shape memory alloy. *Materials Research*. 2005;8:169-172. doi:https://doi.org/10.1590/S1516-14392005000200014.

[36] S. MOHAMMED, F. DAĞDELEN and I. N. QADER. Effect of Ta Content on Microstructure and Phase Transformation Temperatures of Ti75. 5-Nb25. 5 (% at.) Alloy. *Gazi University Journal of Science*.1-1. doi:https://doi.org/10.35378/gujs.947678.